 DOI: 10.1002/masy.201650029

Experimental Investigation of Dynamic Fracture Behaviors of Polymethyl Methacrylate

Guiyun Gao,[1,2] *Jie Zhou*,[1] *Zheng Li**[1]

Summary: Dynamic fracture of polymers plays a vital role in engineering applications. Dynamic fracture behaviors of polymethyl methacrylate were studied using the optical method of caustics. Semi-circular bending specimens were chosen for mixed-mode fracture and crack interaction analysis. The crack initiation, crack propagation, stress intensity factor, and fracture toughness were obtained by analyzing the specke patterns captured during dynamic loading by high-speed imaging techniques. The crack interactions of two symmetric and asymmetric cracks and the influence of damage, including the presence of holes and microcracks on or near the crack path, are discussed. The results show that two cracks on a specimen compete and interact with each other, and lead to the final fracture mode of the specimens. Holes and microcracks on or near the crack path influence the crack path and the crack propagation velocity. The results obtained in this paper could be extended to brittle fracture analysis of materials with multiple cracks or inclusions.

Keywords: crack interaction; fracture; optical method of caustics; semi-circular bending; toughness

Introduction

Polymethyl methacrylate (PMMA) is one of the most widely used polymers in engineering applications. Fracture is, however, unavoidable during application under loading, especially under dynamic loads, and it is therefore important to know how this material fails under all conditions. The process of brittle fracture under mixed-mode loading is more complicated than the traditionally studied fracture under pure mode-I fracture loading, especially under dynamic-loading conditions. The fracture process becomes even more complicated and unpredictable if damage occurs with multiple cracks or in the presence of holes and microcracks.

Semi-circular bend (SCB) specimens are widely used in fracture analysis of brittle materials owing to their simple geometry and loading conditions and the fact that they are easy to machine. These specimens were first proposed for fracture tests of rocks and other brittle materials in 1984 by Chong and Kuruppu,[1] and were adopted by many researchers who used notched SCB specimens to determine the fracture toughness of brittle materials, such as rocks, under either quasi-static or dynamic loading conditions.[2–5] Application of these specimens for studying interactions between a crack and material damage is rare, but very promising.

Crack interaction readily occurs when there are two or more cracks in an engineering structure. Wong et al.[6] observed three-dimensional (3D) surface crack propagation and interactions in PMMA during uniaxial tests that fabricated multiple cracks. Gope et al.[7] experimentally observed bi-crack initiation in a rectangular aluminum structure and predicted the crack growth direction

[1] State Key Laboratory of Turbulence and Complex Systems and College of Engineering, Peking University, Beijing 100871, China
E-mail: lizheng@pku.edu.cn
[2] Institute of Mechanics, Chinese Academy of Sciences, Beijing 100190, China

using an artificial neural network method. Farahmand and Raftopoulos[8] studied the stress intensity factor (SIF) change as a function of pre-crack length and distance in thin plates with parallel and symmetric edge cracks. Theocaris[9] investigated collinear symmetric and anti-symmetric crack interaction and obtained the SIF of each crack. Arakawa et al.[10] studied the SIF, crack growth velocity, and acceleration in a PMMA plate with two holes and one edge crack. Yao et al.[11] experimentally studied the crack growth and interaction of two biased parallel cracks in PMMA using the method of caustics. However, all these studies concerned crack propagation under static-loading conditions. Crack interactions under dynamic loading are more complicated than under static loading and reliable methods need to be developed to evaluate these interactions.

The method of caustics is an important technique in fracture mechanics that allows the dynamic study of fractures.[12–14] This method is sensitive to stress gradients and has a high degree of accuracy. In 1964, Manogg[15] used this method to study fracture for the first time. Theocaris[16] then used this technique to study the size of the plastic zone around the crack tip, the position of the crack tip, and the SIFs. Ma[17] analyzed the transient stress field of stationary cracks. Liu[18] deduced the dynamic SIFs of a mixed-mode propagating crack. Yao analyzed the stress singularities in orthotropic composite materials with mode-I cracks[19] and laminated composites under concentrated loads.[20] Kawagishi[21] evaluated the experimental stress field around the crack tip using this method. The method of caustics is now recognized as an effective technique to study the stress field around the crack tip for different loading conditions.[22,23] In this method, data, which are used for calculating SIFs, are collected only in the tiny area around the crack tip and there is no need for any information pertaining to the applied force or boundary conditions. In addition, the calculation process is easier than that of any other optical method.

In this paper, the dynamic fracture behavior of PMMA is reported. Crack propagation and crack interactions with damage were considered in SCB specimens. The dynamic process of crack initiation and propagation was evaluated using the method of caustics combined with a high-speed photography system. The crack length, the crack propagation velocity, the SIF, and the energy release rate were evaluated. In addition to crack propagation, crack interactions with damage in the sample were analyzed.

Principle of the Dynamic Method of Caustics

The method of caustics is one of the most important techniques in fracture mechanics to evaluate cracks and the deformation zone adjacent to a crack tip, especially for dynamic fractures. This method is based on local deformation around the crack tip, and uses the simple deformation of this zone and optics to characterize the stress or strain concentration during static or dynamic loading.

Figure 1 shows the principle of the method. When a specimen is under load, the thickness and/or refractive index of the specimen will change observably and asymmetrically in the stress singularity zone around the crack tip. As shown in Figure 1, parallel light is refracted when passing through the specimen and an enveloping surface is formed in the space behind the specimen, which is called the caustics surface.

Figure 2 shows the light path and the geometrical effect used in the method of

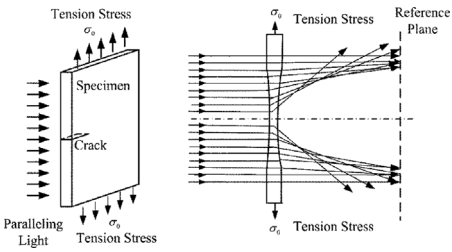

Figure 1.
Principle of the method of caustics.

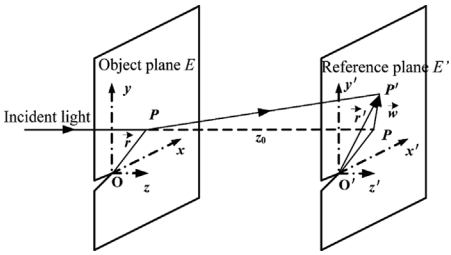

Figure 2.
The light path and geometrical theory used in the method of caustics.

caustics. One can evaluate the mathematical relationship between the observed caustics curve and different parameters of the local deformation and loading using this understanding and the assumed deformation of the material.[24] The equation of the caustics curve can be written as:

$$\mathbf{r}' = \lambda_m \mathbf{r} - z_0 dc \nabla(\sigma_{11} + \sigma_{22}) \tag{1}$$

where $\mathbf{r}'$ and $\mathbf{r}$ represent radius vectors on the reference and object planes, respectively, λ_m represents the optical amplification factor (which equals 1 for the parallel light used in this work), z_0 is the distance between the object and reference planes, d is the thickness of the specimen, c is the optical stress coefficient, and σ_{11} and σ_{22} are the normal stresses on the point P.

The Jacobian matrix of Eq. (1) must vanish because the observed caustics curve is a singular curve (i.e., it represents the point of convergence of many rays of light). This is written as:

$$\mathbf{J}(x,y) = \begin{vmatrix} \dfrac{\partial x'}{\partial r} & \dfrac{\partial x'}{\partial \theta} \\ \dfrac{\partial y'}{\partial r} & \dfrac{\partial y'}{\partial \theta} \end{vmatrix} = 0 \tag{2}$$

Using the mixed-model stress distribution around the crack tip given by Nishioka[25] and Rosakis,[26] we derive the equation for the caustics curve for mixed-mode fracture as:

$$\sigma_{11} = \frac{K_{\mathrm{I}}^d(t)}{\sqrt{2\pi}} B_{\mathrm{I}}(v) \left\{ (2\alpha_l^2 - \alpha_s^2 + 1) \frac{\cos\frac{\theta_l}{2}}{r_l^{1/2}} - \frac{4\alpha_l\alpha_s}{(1+\alpha_s^2)} \frac{\cos\frac{\theta_s}{2}}{r_s^{1/2}} \right\} - \frac{K_{\mathrm{II}}^d(t)}{\sqrt{2\pi}} B_{\mathrm{II}}(v) \left\{ (2\alpha_l - \alpha_s^2 + 1) \frac{\sin\frac{\theta_l}{2}}{r_l^{1/2}} - (1+\alpha_s^2) \frac{\sin\frac{\theta_s}{2}}{r_s^{1/2}} \right\} \tag{3}$$

$$\sigma_{22} = \frac{K_{\mathrm{I}}^d(t)}{\sqrt{2\pi}} B_{\mathrm{I}}(v) \left\{ -(\alpha_s^2 + 1) \frac{\cos\frac{\theta_l}{2}}{r_l^{1/2}} + \frac{4\alpha_l\alpha_s}{(1+\alpha_s^2)} \frac{\cos\frac{\theta_s}{2}}{r_s^{1/2}} \right\} - \frac{K_{\mathrm{II}}^d(t)}{\sqrt{2\pi}} B_{\mathrm{II}}(v) \left\{ -(\alpha_s^2 + 1) \frac{\sin\frac{\theta_l}{2}}{r_l^{1/2}} + (1+\alpha_s^2) \frac{\sin\frac{\theta_s}{2}}{r_s^{1/2}} \right\} \tag{4}$$

where $r_l e^{i\theta_l} = z_l = x_l + i\alpha_l x_2$, $r_s e^{i\theta_s} = z_s = x_s + i\alpha_s x_2$, $\alpha_l = \left(1 - \frac{v^2}{c_l^2}\right)^{1/2}$, $\alpha_s = \left(1 - \frac{v^2}{c_s^2}\right)^{1/2}$, $B_{\mathrm{I}} = (1+\alpha_s^2)/\{4\alpha_l\alpha_s - (1+\alpha_s^2)^2\}$, $B_{\mathrm{II}} = 2\alpha_s/\{4\alpha_l\alpha_s - (1+\alpha_s^2)^2\}$, v is the speed of crack propagation, K_{I}^d and K_{II}^d are the dynamic SIFs for modes I and II, respectively, and C_l and C_s are, respectively, the speeds of the longitudinal and transverse waves.

By substituting Eqs. (3) and (4) into Eq. (1), and based on Eq. (2), the equations

for the relationship between the caustics and initial curves are:

$$\left.\begin{aligned} x' &= r_l\cos\theta_l + \frac{2}{3}\lambda Q(v) r_l^{-\frac{3}{2}}\left\{\beta_{\mathrm{I}}\cos\frac{3}{2}\theta_l - \beta_{\mathrm{II}}R(v)\sin\frac{3}{2}\theta_l\right\} \\ y' &= \frac{r_l}{\alpha_l}\sin\theta_l + \frac{2}{3}\alpha_l\lambda Q(v) r_l^{-\frac{3}{2}}\left\{\beta_{\mathrm{I}}\sin\frac{3}{2}\theta_l + \beta_{\mathrm{II}}R(v)\cos\frac{3}{2}\theta_l\right\} \end{aligned}\right\} \quad (5)$$

and

$$r_l = Q^{\frac{2}{5}}(v)H \quad (6)$$

where

$$Q(v) = B_{\mathrm{I}}(v)(\alpha_l^2 - \alpha_s^2),\ R(v) = \frac{B_{\mathrm{II}}(v)}{B_{\mathrm{I}}(v)},$$

$$\beta_{\mathrm{I}} = \frac{K_{\mathrm{I}}^d}{\sqrt{\left(K_{\mathrm{I}}^d\right)^2 + \left(K_{\mathrm{II}}^d\right)^2}},$$

$$\beta_{\mathrm{II}} = \frac{K_{\mathrm{II}}^d}{\sqrt{\left(K_{\mathrm{I}}^d\right)^2 + \left(K_{\mathrm{II}}^d\right)^2}},$$

$$\mu = -\frac{3}{2\sqrt{2\pi}}cdz_0\left\{\left(K_{\mathrm{I}}^d\right)^2 + \left(K_{\mathrm{II}}^d\right)^2\right\},$$

$$A = \mu^2\alpha_l^2\left(\beta_{\mathrm{I}}^2 + \beta_{\mathrm{II}}^2R^2(v)\right),$$

$$B = \mu\left(1-\alpha_l^2\right)\left\{\beta_{\mathrm{I}}\cos\frac{5}{2}\theta_l + \beta_{\mathrm{II}}R(v)\cos\frac{3}{2}\theta_l\right\},$$

$$H = \left(\frac{-B+\sqrt{B^2+4A}}{2}\right)^{\frac{5}{2}}.$$

The relationship between the static SIF and the size of caustics patterns can be derived from previous work[18] as:

$$K_{\mathrm{I}} = \frac{2\sqrt{2\pi}}{3d|c|z_0(1+\tan^2\alpha)^{1/2}}\left\{\frac{D_t}{\frac{10}{3}\sin\frac{2}{5}\pi\cos\frac{2}{5}\alpha}\right\}^{5/2}$$
$$K_{\mathrm{II}} = K_{\mathrm{I}}\tan\alpha \quad (7)$$

where $|\alpha| = \frac{5}{2}\arctan\left\{[2\sin\frac{2}{5}\pi - \eta(1+\cos\frac{\pi}{5})]/\eta\sin\frac{\pi}{5}\right\}$, $\eta = D_t/D_l$. D_t and D_l are, respectively, the transverse and longitudinal diameters of the shadow pattern. The relationship between the static and dynamic SIFs is $K_{\mathrm{I}}^d = Q^{-1}(v)K_{\mathrm{I}}$. At room temperature, the stress wave velocity of the longitudinal wave in PMMA is about 2700 m/s while the velocity of the transverse wave is about 1300 m/s. During the experiment, the velocity of the crack propagation is about 250 m/s. This allows us to calculate $Q(v) = 1.013$, which shows that the velocity has only a small influence on the dynamic SIF.

Dynamic Fracture Experiments Using the Method of Caustics

In this series of experiments, SCB specimens made of PMMA were used. Figure 3 shows the shapes of the SCB specimens that were used to study the basic fracture modes and crack interactions.

The transmitted method of caustics was used because the specimens are transparent. The setup of the dynamic transmitted light caustic method is schematically shown in Figure 4. This includes a DDGS-II, multi-spark, high-speed photography system (modified Cranz–Shardin high-speed photography system), a time-control system, and a loading system. The DDGS-II system consisted of 16 point lights and 16 cameras

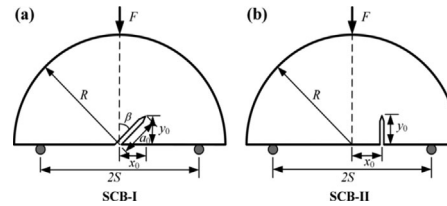

Figure 3.
Schematics of crack profiles for different SCB specimens: (a) SCB-I, (b) SCB-II.

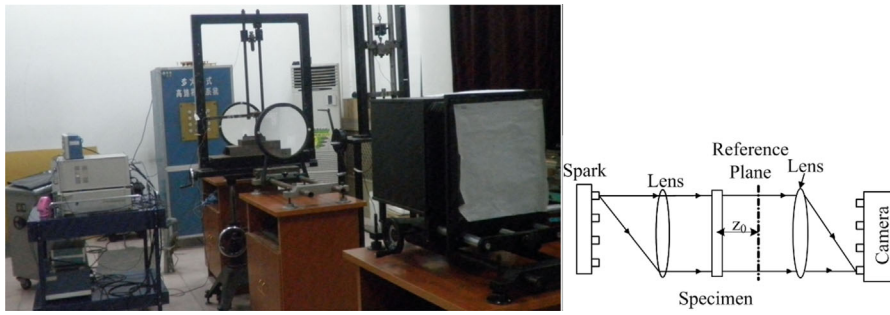

Figure 4.
High-speed multi-spark photography system.

that could record 16 frames of caustic patterns for each dynamic fracture experiment. The trigger time and interval of each frame were designed and set using the time-control system. A dynamic impact was applied using a drop-tower loading system that used a 0.68-kg weight and was 374 mm high (loading velocity of 2.71 m/s). A typical load pulse obtained is shown in Figure 5.

Results and Discussion

Dynamic Fracture of PMMA Under Dynamic Loading

A typical caustic pattern and its evolution in a dynamic fracture process are shown in Figure 6. The time on the photographs is the time interval that is recorded from triggering the load. Initially, the diameter of the caustic pattern increased with time, while the crack tip position did not change. When the caustic pattern reached its maximum size, just before 196 μs, the crack propagation initiated. At this point, the shadow pattern became unstable and the crack grew rapidly until the specimen broke. Similar characteristics were observed during the dynamic fracture process for other specimens with different crack positions and angles. The SIFs were calculated for each time interval using the caustic patterns. In these experiments, the optical stress coefficient c of PMMA was -0.88×10^{-9} m/N and the distance z_0 between the specimen and the reference plane was 440 mm. The fracture toughness of PMMA is about $1.2\,\mathrm{MPa} \cdot \mathrm{m}^{1/2}$.

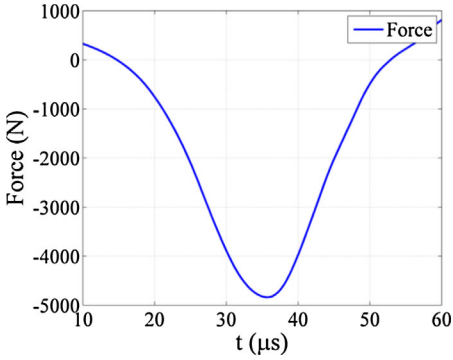

Figure 5.
Typical load history during drop tower loading.

Crack Interaction Between Two Cracks Under Dynamic Load

The crack interaction between two cracks under dynamic load was studied. SCB specimens with offset parallel cracks were chosen to study the interactions of symmetric and asymmetric cracks. The position of the crack noted as Crack 1 was $x_0 = 28.10$ mm, $y_0 = 16$ mm and that noted as Crack 2 was at $x_0 = 28.10$ mm, $y_0 = 16$ mm, where the origin of the coordinate is the center of the circle, as shown in Figure 3. Figure 7 shows the caustic patterns of the two symmetric cracks as they changed with loading time. We observe stress concentration on both crack tips; at 264 μs, both cracks began to propagate at almost at the same time. The velocities of crack propagation of these two cracks, which can be

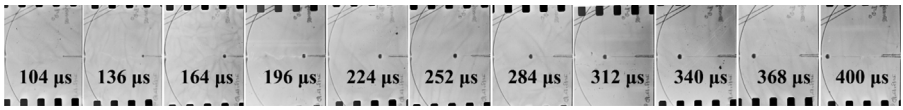

Figure 6.
Typical caustic shadow pattern evolution with time during dynamic fracture process.

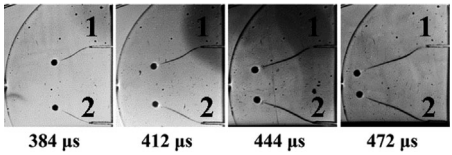

Figure 7.
Fracture process of specimen with symmetric cracks.

acquired from Figure 8, were 267.2 m/s and 263.4 m/s, respectively, and the difference in velocity was only 1.4%. Figure 8(b) shows the mode-I and -II SIFs of the two cracks. The SIFs of the two modes are difficult to analyze. For this, we used the energy release rate:

$$G_e = \frac{K_{eff}^2}{E'} = \frac{1}{E'}\left(K_I^2 + K_{II}^2\right) \tag{8}$$

where E' is the equivalent elastic modulus and K_{eff} is the equivalent SIF. In a plane stress problem, E' is equal to the elastic modulus.

As shown in Figure 8(c), the energy release rates of the two cracks have almost the same value, which demonstrates that, for symmetric cracks under symmetric loading, we see similar dynamic fracture. The crack paths of the two cracks are also similar to each other, as Figure 8(d) shows.

The interaction of asymmetric cracks was also analyzed. As given in Table 1, the positions of the crack tips were different. The caustic patterns are shown in Figure 9. Compared with those in Figure 6, the caustic patterns in Figure 9 have obvious differences and the propagation of Crack 1 was faster than that of Crack 2. At the beginning of loading, the caustic patterns of

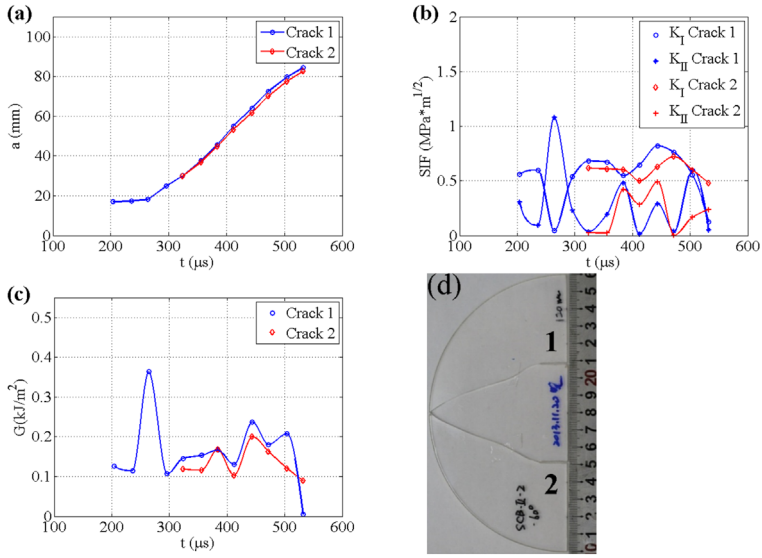

Figure 8.
Fracture of symmetric cracks under symmetric loading: (a) crack lengths *a* vs. time *t*; (b) SIFs of two cracks vs. time *t*; (c) energy release rate *G* vs. time *t*; (d) the specimen after fracture.

Table 1.
Parameters of asymmetric cracks.

Crack no.	x_0 [mm]	y_0 [mm]	Initiation time [μs]	Propagation velocity [m/s]
Crack 1	27.92	15.7	284	328.29
Crack 2	28.20	16.3	312	200.51
Differences	0.99%	3.68%	9.86%	38.9%

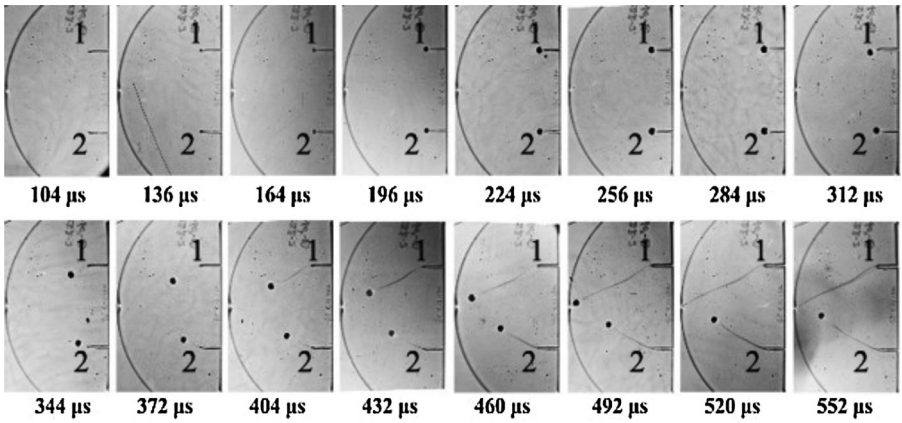

Figure 9.
Fracture process of specimen with asymmetric cracks.

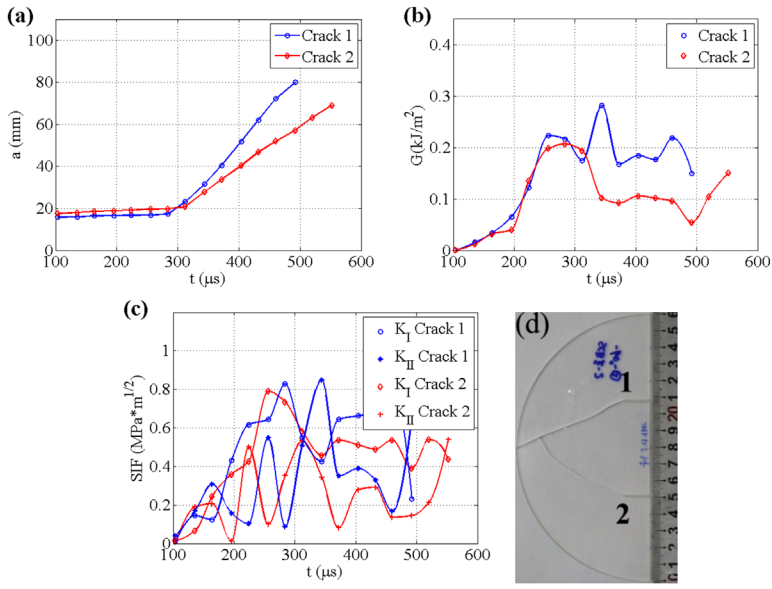

Figure 10.
Fracture results for asymmetric cracks: (a) crack lengths *a* vs. time *t*; (b) energy release rate *G* vs. time *t*; (c) SIFs of two cracks vs. time *t*; (d) the specimen after fracture.

Table 2.
Parameters of specimens with one or several holes.

Specimen type	No.	β	a_0 [mm]	Hole position y_1 [mm]	Hole diameter Φ [mm]
One hole	SCBII-0-1Hole	0°	19.9	21.5	1.4
Multiple holes	SCBII-0-8Holes	0°	20.8	20.9~26.7	1.2

the two cracks grew; Crack 1 initiation occurred at 284 μs, while the caustic pattern of Crack 2 continued to grow and only propagated 28 μs later. The two cracks propagated until the specimen broke into three pieces (as shown in Figure 10(d)).

Figure 10 further analyzes these caustic patterns. The differences in propagation velocities are shown in Figure 10(a). The propagation velocity of Crack 1 was 328.29 m/s, while that of Crack 2 was 200.51 m/s. The small difference (0.99–3.68%) in crack fabrication led to about 9.86% difference in initiation time for crack propagation and 38.9% difference in crack propagation velocity. The SIFs in Figure 10(c) are more complicated than that of the symmetric cracks and the energy release rate of Crack 1 was larger than that of Crack 2, which caused Crack 1 to propagate first. The path of crack propagation is shown in Figure 10(d) and is also asymmetric.

Influence of Holes

The influence of small holes on crack propagation was studied for single and multiple holes. The parameters of the specimens with holes are listed in Table 2.

The crack propagation path in the specimen with a single hole, as shown in Figure 11(a), was a typical path of mode-I fracture and was not influenced by the hole; however, the crack propagation velocity near the hole was affected by the hole, as shown in Figure 11(b), and crack arrest occurred. The crack propagation started at 156 μs and the crack tip almost arrested for up to 20 μs when the crack tip

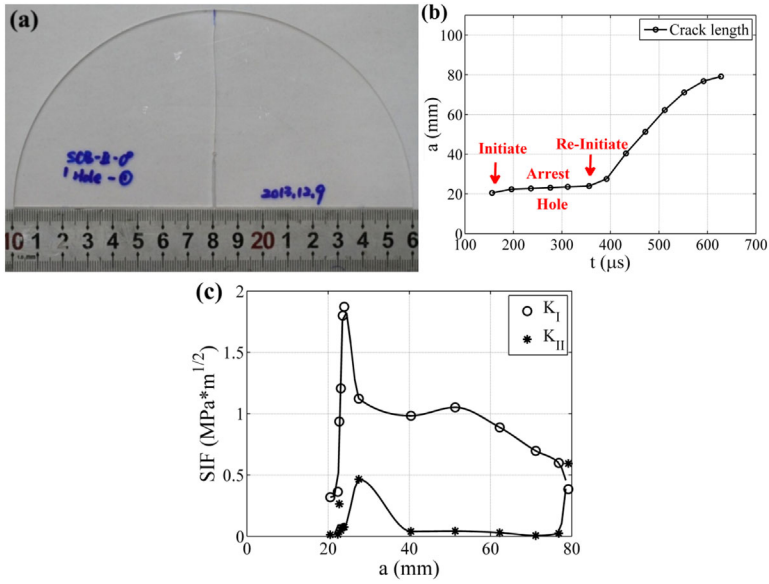

Figure 11.
Fracture results of specimen with a single hole: (a) fractured specimen; (b) crack length a vs. time t; (c) SIFs of two cracks vs. crack length a.

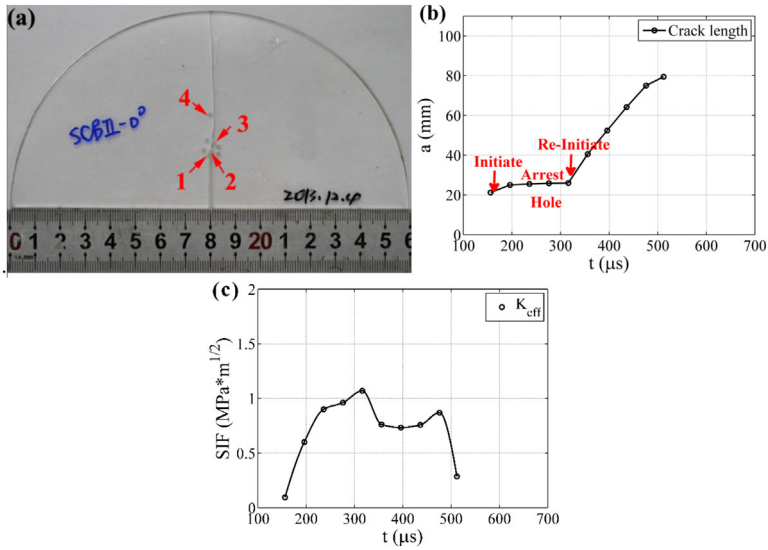

Figure 12.
Fracture results of specimen with eight holes: (a) fractured specimen; (b) crack lengths a vs. time t; (c) equivalent SIF K_{eff} vs. time t.

approached the hole. During this stage, the SIF of the crack tip continued to increase to a threshold of $1.87\,\mathrm{MPa}\cdot\mathrm{m}^{1/2}$, which was much larger than the crack initiation value and results from the existence of the hole shown in Figure 11(c). After the arrest, the crack propagation velocity increased and reached 249.6 m/s, which is the normal mode-I fracture propagation velocity for this specimen.

If multiple holes appeared near the crack propagation path, as shown in Figure 12(a), the crack propagation path deviated from that in Figure 11(a). Two deviations occurred when the crack passed the multiple-hole region and the crack stopped for about 120 μs around hole 2 (Figure 12). When K_{eff} reached $1.07\,\mathrm{MPa}\cdot\mathrm{m}^{1/2}$, the crack re-initiated its motion and the velocity reached 365.7 m/s. During dynamic fracture, holes near the crack path can therefore slow down crack propagation: for example, near hole 4, the velocity decreased from 365.7 m/s to 287.1 m/s (about 21.5%) and the path also deviated toward the holes (Figure 12(a)).

If a single hole occurred in the propagation path of a SCB-II specimen, shown in Figure 13(a), the crack still arrested near

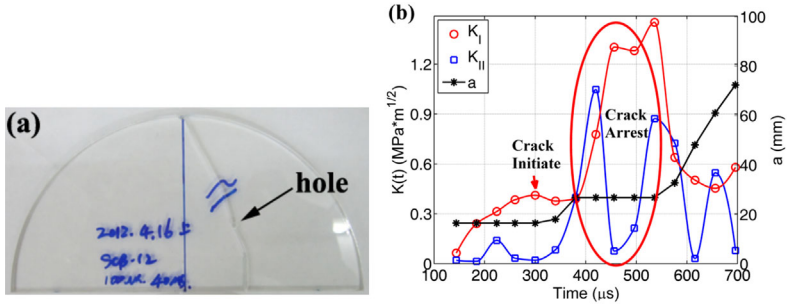

Figure 13.
Fracture results of SCB-II specimen with one hole on the path: (a) specimen after fracture; (b) SIFs and crack length vs. time t.

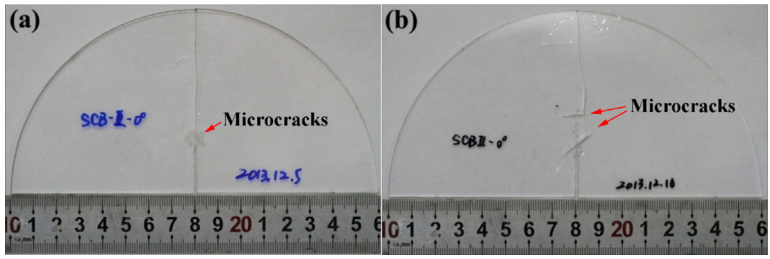

Figure 14.
Dynamic fracture of specimens with two type microcracks: (a) microcracks-1 specimen; (b) microcracks-2 specimen.

the hole, as shown in Figure 13(b). The propagation velocity of the crack increased by about 50% (from 219.6 m/s to 329.2 m/s) and the crack path deviated from the original path.

All of these experiments demonstrate that a hole on or near the propagation path of a crack can stop the propagation or change the propagation velocity of the crack and can deviate the path toward the hole.

Interaction Between Microcracks and Crack Propagation

Two types of microcracks, shown in Figure 14, were chosen to study the influence microcracks on crack propagation. Compared with

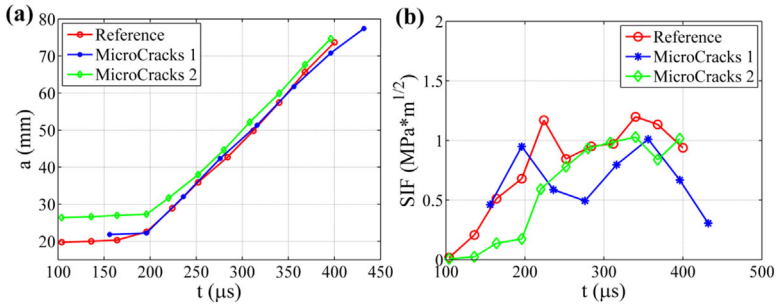

Figure 15.
Propagation in specimens with two types of microcracks: (a) crack length *a* vs. time *t*; (b) SIFs vs. time *t*.

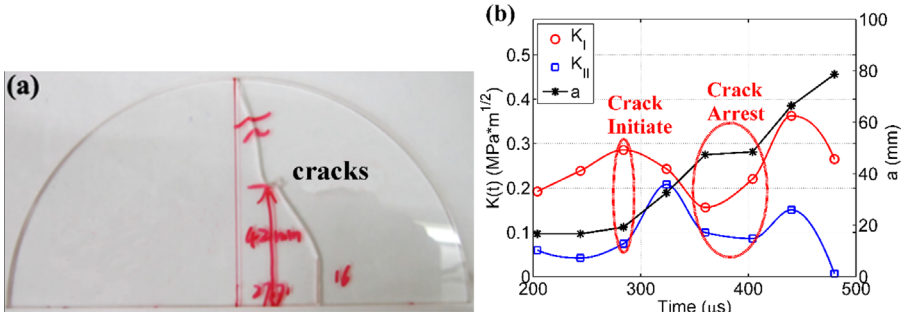

Figure 16.
Fracture results of SCB-II specimen with microcracks: (a) specimen after fracture; (b) SIFs and crack length *a* vs. time *t*.

a specimen without microcracks, the time of crack initiation was delayed by several microseconds, as shown in Figure 15(a). The crack propagation velocities of specimens with microcracks were 237.0 m/s and 240.6 m/s, while that of the specimen without microcracks was 251.3 m/s. The crack propagation velocity decreased by about 4.3–5.7%. The largest SIF value measured for specimens with microcracks was smaller than for those without microcracks.

For the offset crack specimen (labeled as SCB-II), the same conclusion was obtained, as shown in Figure 16. Crack propagation was delayed by microcracks positioned around the crack path, and the crack propagation velocity decreased by about 17.3% from 370.3 m/s to 306.1 m/s.

Conclusion

In this study, the caustic method was developed and applied to study dynamic fracture behaviors of PMMA. Equations for the caustics curve were derived. In addition, the relationship between the size of the caustic shadow patterns and the SIFs was obtained.

Experiments were conducted to investigate the fracture properties and crack interaction with damage zones, such as other cracks, holes, and microcracks.

Results show that parallel cracks compete and interact with each other until one of them dominates failure of the specimen. The fracture of parallel cracks is more difficult to initiate than that of a single crack and the accumulation of energy determines which crack starts moving first. Small differences in a pre-crack tip position (1–3%) can lead to about 9.86% and 38.9% difference in initiation time and velocity of crack propagation, respectively. Holes have a small influence on the crack path, but temporarily obstruct the crack propagation. Tiny cracks and holes near the crack have an obvious influence on the crack propagation path and crack propagation velocity. They can stop the propagation or change the propagation velocity of the crack by 5–50% and cause the crack to deviate from its path.

Acknowledgements: This work was supported by the National Basic Research Program of China under Grant No. 2010CB731503.

[1] K. P. Chong, M. D. Kuruppu, *Int. J. Fract.* **1984**, *26*, R59.
[2] M. R. Ayatollahi, M. R. M. Aliha, M. M. Hassani, *Mat. Sci. Eng. a-Struct.* **2006**, *417*, 348.
[3] M. D. Kuruppu, K. P. Chong, *Eng. Fract. Mech.* **2012**, *91*, 133.
[4] R. Chen, K. Xia, F. Dai, F. Lu, S. N. Luo, *Eng. Fract. Mech.* **2009**, *76*, 1268.
[5] F. Dai, K. Xia, H. Zheng, Y. X. Wang, *Eng. Fract. Mech.* **2011**, *78*, 2633.
[6] R. H. C. Wong, C. M. Law, K. T. Chau, W.-S. Zhu, *Int. J. Rock Mech. Min. Sci.* **2004**, *41*, 360.
[7] D. Gope, P. C. Gope, A. Thakur, *Int. J. Struct. Integ.* **2013**, *4*, 321.
[8] B. Farahmand, D. D. Raftopoulos, *Eng. Fract. Mech.* **1981**, *14*, 439.
[9] P. Theocaris, *J. Strain. Anal. Eng.* **1972**, *7*, 186.
[10] K. Arakawa, T. Mada, K. Takahashi, *Int. J. Fract.* **2000**, *105*, 311.
[11] X. F. Yao, W. Xu, M. Q. Xu, K. Arakawa, T. Mada, K. Takahashi, *Polym. Test.* **2003**, *22*, 663.
[12] K.-H. Lee, J.-S. Hawong, S.-H. Choi, *Eng. Fract. Mech.* **1996**, *53*, 119.
[13] X. F. Yao, H. P. Zhao, H. Y. Yeh, *J. Reinf. Plast. Comp.* **2005**, *24*, 657.
[14] K. Ravi-Chandar, W. G. Knauss, *Int. J. Fract.* **1984**, *25*, 247.
[15] P. Manogg, in "*Schattenoptische messung der spezifischen bruchenergie wahrenddes bruchvorgangs bei Plexiglas*", Proc. Int. Conf. Physics Non-Crystalline Solids Delft, The Netherlands p. 481.
[16] P. S. Theocaris, *Appl. Optics* **1971**, *10*, 2240.
[17] C.-C. Ma, S.-K. Chen, *Int. J. Fract.* **1992**, *58*, 345.
[18] S. Huang, S.-N. Luo, B. S. A. Tatone, K. Xia, *J. Mech. Mater. Struct.* **2011**, *6*, 813.
[19] X. F. Yao, J. D. Chen, G. C. Jin, K. Arakawa, K. Takahashi, *Compos. Sci. Technol.* **2004**, *64*, 917.
[20] X. Yao, W. Xu, M. Xu, G. Jin, H. Yeh, *Int. J. Solids Struct.* **2004**, *41*.
[21] Y. Kawagishi, M. Shozu, Y. Hirose, *Mech. Mater.* **2001**, *33*, 741.
[22] G. Y. Gao, Z. Li, J. Xu, *Opt. Lasers Eng.* **2011**, *49*, 632.
[23] X. F. Yao, W. Xu, *Fatigue Fract. Eng. Mater. Struct.* **2011**, *34*, 448.
[24] J. Beinert, J. Kalthoff, in *Experimental Evaluation of Stress Concentration and Intensity Factors*, G. C. Sih, Ed., Springer, Netherlands, **1981**, p. 281.
[25] T. Nishioka, S. N. Atluri, *Eng. Fract. Mech.* **1983**, *18*, 1.
[26] A. J. Rosakis, *Eng. Fract. Mech.* **1980**, *13*, 331.

